

## Application of Eco-friendly Magnetite Nanoparticles Coated with Rosin Amidoxime as Corrosion Inhibitor for Mild Steel in 1 M Hydrochloric Acid Solution

Ayman M. Atta<sup>1,2\*</sup>, Gamal A. El-Mahdy<sup>1,3\*</sup>, Hamad A. Al-Lohedan<sup>1</sup> and Sami A. Al-Hussain<sup>1,4</sup>

<sup>1</sup> Surfactants research chair, Department of Chemistry, College of Science, King Saud University, Riyadh 11541, Kingdom of Saudi Arabia.

<sup>2</sup> Egyptian Petroleum Research Institute, 1 Ahmad Elzomor St., Nasr city 11727, Cairo, Egypt.

<sup>3</sup> Chemistry department, college of science, Helwan university, Helwan, Cairo, Egypt

<sup>4</sup> Faculty of science, Department of Chemistry, Al-Imam Muhammad Bin Saud Islamic University, Riyadh 11632, Kingdom of Saudi Arabia.

\*E-mail: [aatta@ksu.edu.sa](mailto:aatta@ksu.edu.sa)

*Received:* 21 November 2014 / *Accepted:* 18 December 2014 / *Published:* 19 January 2015

---

In the present study, new magnetite nanoparticles coated with rosin amidoxime prepared to apply as corrosion inhibitors for steel in 1 M HCl. Rosin amidoxime was prepared from hydrolysis of rosin-acrylonitrile Diels Alder adduct using hydroxylamine in basic medium. A new monodisperse magnetite nanoparticles was prepared by a simple and inexpensive co-precipitation method followed by capping with rosin amidoxime. The chemical structure, particle size and morphology of magnetite capped with rosin amidoxime were characterized by Fourier transform infrared spectroscopy (FTIR), transmission electron microscopy (TEM), and dynamic light scattering (DLS). Corrosion protection properties of magnetite-RK/amidoxime nanoparticles on steel in hydrochloric acid have been studied by polarization and electrochemical impedance spectroscopy (EIS). The results show that magnetite-RK/amidoxime nanoparticles acts as good inhibitor and inhibition efficiency (%IE) increases with inhibitor concentration. Potentiodynamic polarization measurements indicated that magnetite-RK/amidoxime nanoparticles acts as a mixed type inhibitor. EIS results indicated that the charge transfer resistance ( $R_{ct}$ ) increases with magnetite-RK/amidoxime concentration. IE values obtained from potentiodynamic polarization showed a reasonable agreement with those obtained from EIS measurements.

---

**Keywords:** Magnetite-RK/amidoxime nanoparticles, Acid, corrosion, Polarization, steel, EIS, inhibition

## 1. INTRODUCTION

Iron and its alloys play an important role in petroleum fields which used for production, storage, transportation and processing of petroleum crude oil and natural gases due to its particular properties (excellent thermal and electrical conductivity, malleability, ductility, etc.). The petroleum crude oil and products contain several corrosive materials included acids, salts, water organic and inorganic derivatives which contaminated with crude oil during production [1]. There are several materials were used as corrosion inhibitors or organic coatings to protect iron from corrosion [2]. In general, organic compounds are effective inhibitors of aqueous corrosion of many metals and alloys. The highly anticorrosion materials for iron are called self-assembled materials (SAMs). The ordered and stable SAMs [3] which form spontaneously by chemical adsorption on metal surface can prevent corrosive ions from transferring to the metal surface so that it can protect the metal from corrosion effectively [4,5]. The requirements for production of new and effective corrosion inhibitors included the high performance at low concentrations, high temperature and its effect on the environment. In our previous works [6-12] we used metal and metal oxide nanoparticles as core coated with biopolymers as shell to prepare self-assembled monolayer at iron surfaces to protect from the corrosive environment. These materials showed high performance to protect iron from corrosion at low concentrations.

Rosin as biomaterial contains hydrophobic moiety attracted more attention in our previous works to prepare water soluble surfactants or to modify their chemical structure to use as organic coatings [13-19]. Oxime compounds have good solubility in water and are of nontoxic and biodegradable contain the characteristic functional group of C=N-OH with electronegative N, O atoms and double bond simultaneously [20, 21], this makes the investigation of their inhibiting properties significant in the context of the current priority to produce eco-friendly inhibitors. It was previously reported that the oxime compounds have great ability to form self-assembly films on metallic substrate [22]. However, the data regarding the application of oxime derivatives as corrosion inhibitors is very poor. There are some studies used aromatic oxime derivatives as corrosion inhibitors in salt, acidic and alkaline aqueous media [23-25] for aluminum. However, to the best of our knowledge, the literature available to date about oxime compounds as corrosion inhibitors for steel in HCl solution is almost scant. The objective of the present work is to synthesis amidoxime from rosin gum to prepare highly dispersed magnetite nanoparticles using cheap and one step method. The application of magnetite coated amidoxime as self- assembled corrosion inhibitors for steel in acidic medium is another goal of the present investigation.

## 2. EXPERIMENTAL

### 2.1. Materials

Anhydrous FeCl<sub>3</sub> and potassium iodide were purchased from Aldrich chemical Co. Rosin acid [acid number = 184 mg of KOH g<sup>-1</sup>, 99%] were separated and purified by crystallization from cooled and concentrated acetone solutions of commercial rosin (Khangzhou Forest Chemical Plant, Deqing,

China). Hydroxylamine hydrochloride (Fluka), and p-toluene-4-sulfonic acid monohydrate (PTSA; Aldrich) were used as received. Hydroxylamine hydrochloride (40.1 g) was dissolved in 290 ml of methanolic solution (methanol: water 5: 1). The hydroxyl amine was neutralized by sodium hydroxide solution till pH 10 and the precipitated NaCl was removed by filtration. Acrylonitrile AN (Fluka), was purified by distillation under reduced pressure. Distilled AN was stabilized with 0.1% hydroquinone. The dehydro decarboxylation of rosin to prepare Diels–Alder adduct of rosin ketone with acrylonitrile (RK-AN) was efficiently prepared and purified as described previously [19, 26]. The steel sample had the following composition (wt.%): 0.14% C, 0.57% Mn, 0.21% P, 0.15% S, 0.37% Si, 0.06% V, 0.03% Ni, 0.03% Cr and the balance Fe. Before the measurements are taken the samples were abraded using different grades of emery papers then washed with distilled water, degreased with acetone and washed thoroughly with distilled water for many times and quickly immersed into the test solution after drying. The aggressive solutions of 1.0 M HCl were prepared by dilution of analytical grade 37% HCl with distilled water.

## 2.2. Preparation technique

### 2.2.1. Preparation of RK/ amidoxime

The prepared RK-AN (30 g) was reacted with the prepared hydroxylamine solution at 70 °C for two hours. The prepared rosin amidoxime resin was separated by filtration and washed several time by methanolic solution then treated with 0.1 M HCl solution for at least 5 min. Finally, resin was filtered and washed several times by methanolic solution and dried at 50 °C to constant weight.

### 2.2.2. Preparation of magnetite coated RK/amidoxime nanoparticle:

Potassium iodide (13.2 g, 0.08 mol) dissolved in distilled water (50 mL) and anhydrous FeCl<sub>3</sub> (40 g) dissolved in distilled water (300 mL) were stirred together at room temperature for one hour under N<sub>2</sub> atmosphere until iodine precipitated in the solution. RK/ amidoximes (10 g) was solubilized in ethanol-water solvent (100 mL, 4:1 vol%) and added dropwise to the reaction mixture (included iodine as precipitate) at the same time as 25% ammonia solution (200 mL). The reaction mixture was then gently warmed to 45 °C under stirring and N<sub>2</sub> bubbling for 4 h until black magnetite was formed as colloidal solution. The magnetite was collected using ultracentrifuge at 8,000 rpm filtered, washed with distilled water, ethanol, dried under vacuum at 30 °C (the precipitate was dried without heating) and weighed. High yield magnetite coated RK/amidoxime nanoparticle 99 % was obtained after filtration and washing with ethanol five times.

## 2.3. Characterization

FTIR spectra were analyzed with a Nicolet FTIR spectrophotometer (city, state abbrev if US, country) using KBr in the wavenumber range of 4000–500 cm<sup>-1</sup> with a resolution accuracy of 4 cm<sup>-1</sup>. All samples were ground and mixed with KBr and then pressed to form pellets.

Transmission electron microscopy (TEM) micrographs were taken with a JEOL JEM-2100F. A few drops of magnetite nanoparticle solution were diluted into 1 mL of ethanol, and the resulting ethanol solution was placed onto a carbon coated copper grid and allowed to evaporate.

Dynamic light scattering (DLS) measurements were performed on a Zetasizer Nano ZS (Malvern Instruments, Malvern, U.K.) with a 633 nm He-Ne laser using ethanol/water (4/1) as solvent. The nanoparticles size was further measured by DLS at 25 °C.

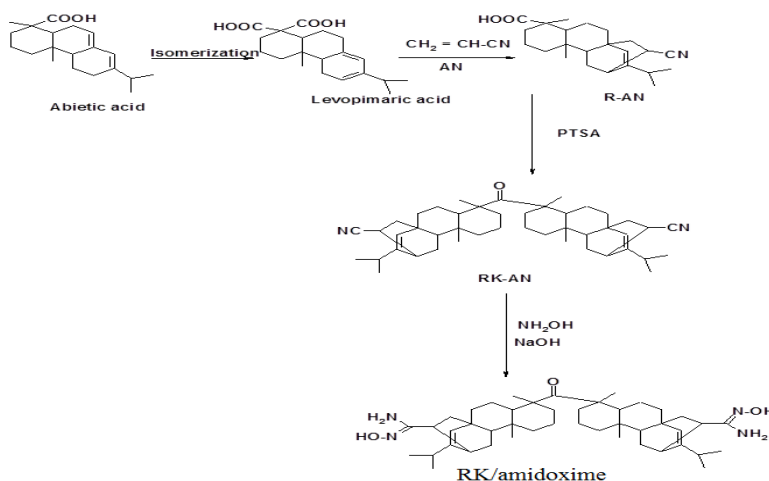
#### 2.4. Electrochemical tests

Electrochemical tests were employed to evaluate the corrosion protection performance of the inhibitor. All electrochemical measurements were performed using a SI 1287 Solartron (potentiostat/galvanostat) and Solartron 1260 as frequency response analyzer. All test were conducted in a conventional three-electrode system. A saturated calomel electrode (SCE), a platinum sheet and the steel samples were used as reference electrode, auxiliary electrode and working electrode, respectively. The potentiodynamic polarization measurements were performed at a constant scan rate of 1 mV/ s. Electrochemical impedance spectroscopy (EIS) plots were obtained in the frequency range from 10 kHz to 10 mHz. Polarization data was analyzed using CorrView and Corr- Ware software, while the impedance data were analyzed using Zplot and ZView software.

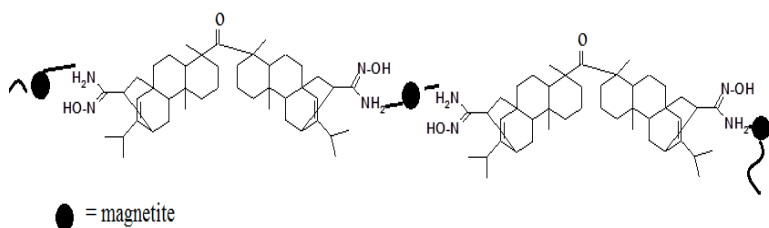
### 3. RESULTS AND DISCUSSION

Rosin acids (RA) have carboxylic acid and conjugated double bond in their hydrophenancerene hydrophobic Skelton. These bonds can react as diene with acrylonitrile (AN) as dienophile to form Diels Alder adduct [26]. The rosin ketone amidoxime can be prepared by dehydro decarboxylation of Diels Alder adduct in the presence of PTSA as catalyst at temperature of 240 °C followed by reaction with hydroxylamine in basic medium as represented in Scheme 1. The cycloaddition reaction between RA and AN was completed by isomerization of abietic acid (the major constituent of RA) into levopimaric acid at and a high reaction temperature (185–190 °C) and with a prolonged reaction duration (10 h) developed with high yields (ca. 95%) [26]. The cyanide functional groups of RK-AN were reacted with hydroxylamine in an alkaline medium to yield amidoxime groups. Herein we will modify the surface of magnetite nanoparticles to prepare new monodisperse magnetite in aqueous medium. In this respect, magnetite was prepared from ferrous and ferric cations which produced from reaction between ferric chloride and potassium iodide as represented in the experimental section. The ferrous and ferric cations were hydrolyzed at low temperature at pH 9 in the presence of iodine to produce iron oxide nanoparticles [27]. Moreover, RK/ amidoxime were used as capping agent to produce dispersed coated magnetite core-shell nanoparticles as illustrated in the scheme 2. It was expected that amidoxime group of RK/ amidoxime can be bonded either with chemical bonding or with physical adsorption of amidoxime derivatives with magnetite surfaces as represented in scheme 2. The chemical bond can be produced with chelation of iron with hydroxyl or amino groups of

amidoxime. The physical adsorption on magnetite nanoparticles with RK/amidoxime can be explained by dipole-dipole interaction mechanism among iron and carbonyl, C=N-OH or amino groups.



**Scheme 1.** Preparation of RK/amidoxime.



**Scheme 2.** Interaction between magnetite and RK/amidoxime.

### 3.1. Chemical structure of magnetite coated with RK/amidoxime

FTIR spectra of RK/ amidoxime and magnetite coated RK/ amidoxime were represented in Figure 1 to verify their chemical structures. FT-IR spectrum RK/amidoxime (figure 1a) shows appearance of new band of amidoxime at  $1656\text{ cm}^{-1}$ , and amide II band of N-H at  $1549\text{ cm}^{-1}$ , respectively and disappearance of the characteristic absorption band at  $2245\text{ cm}^{-1}$  due to CN stretching. The absorption bands of rosin appeared for C-H stretching at  $2936\text{--}2870\text{ cm}^{-1}$ , C=O stretching at  $1707\text{ cm}^{-1}$  and C=C stretching in hydrophenanetherene moiety at  $1462\text{ cm}^{-1}$ . The band at  $932\text{ cm}^{-1}$  may be assigned to the N–O bond of the amidoxime group [28]. The structure of the magnetic capped with RK/amidoxime was characterized by FTIR analysis that represented in Figure 1b. In the previous work [27], FTIR spectrum of uncapped iron oxide confirmed the presence of  $\alpha\text{-Fe}_2\text{O}_3$  (hematite) beside magnetite nanoparticles. Figure 1b confirmed the appearance of a strong absorption band at  $576\text{ cm}^{-1}$  which was assigned to the Fe–O vibration frequency of magnetite. Moreover, the absorption band at  $1652\text{ cm}^{-1}$  (corresponding to the C=N stretching vibrations of amidoxime groups) indicated the

presence of RK/amidoxime. A broad absorption bands was found around 3299 and 3450  $\text{cm}^{-1}$  that attributed to stretching vibration of hydroxyl groups and  $\text{NH}_2$  in the RK/amidoxime molecules. These data indicated that the presence of RK/amidoxime during the formation of magnetite inhibited its air oxidation and produced  $\text{Fe}_3\text{O}_4$  nanoparticles without any formation of other iron oxides.

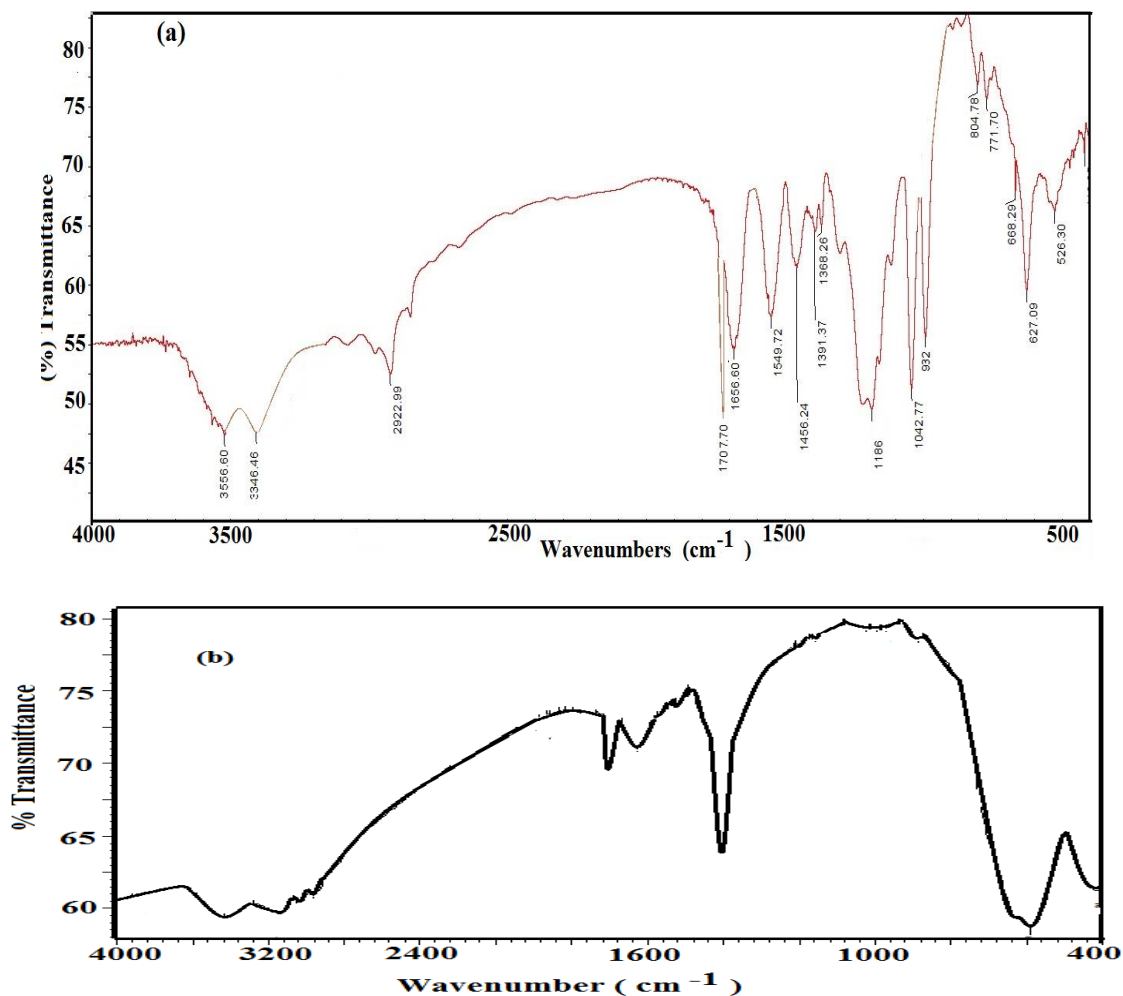


**Figure 1.** FTIR spectra of a) RK/amidoxime and b) magnetite-RK/amidoxime nanoparticles.

### 3.2. Morphology and particle size of magnetite coated with RK/amidoxime

The morphology and microstructure of  $\text{Fe}_3\text{O}_4$  coated with RK/amidoxime were investigated from TEM analysis. Figure 2 shows that the capped  $\text{Fe}_3\text{O}_4$  with RK/ amidoxime has spherical core/shell morphology. The appearance of dark colored  $\text{Fe}_3\text{O}_4$  cores and white gray colored of RK/ amidoxime shells. In our previous work [26], the uncapped  $\text{Fe}_3\text{O}_4$  nanoparticle has particle diameter 6.2 nm while the diameter of  $\text{Fe}_3\text{O}_4$  coated with RK/ amidoxime was 28-42 nm. It can also observe that there is no any magnetite particles appeared without RK/amidoxime coatings. These data indicated that there are strong bonds formed between magnetite and RK/amidoxime.

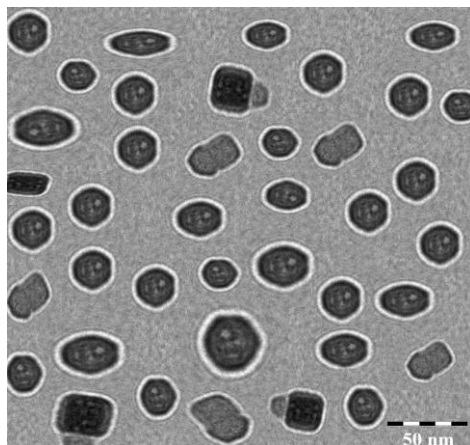


**Figure 2.** TEM micrograph of magnetite-RK/amidoxime nanoparticles.

DLS is one of the most favorable methods used to investigate the size of particles, particle distribution and in monitoring the colloidal stability of MNP suspension [37]. As represented in scheme 2, it was expected that the hydrophilicity of magnetite will be affected by coating with RK/amidoxime based on core-shell morphology due to chelation of magnetite with amidoxime groups. The formation of this bond leads to increase the hydrophobicity of magnetite by hydrophobic hydrophenancere of rosin which will reflect on the aggregation of particles in the water. It was also expected that the RK/amidoxime can be capped around magnetite by both single-layer and bilayer coatings. It is well known that the size distributions and surface charges of the magnetic nanoparticles are key factors for their dispersability and stability in aqueous medium. It was reported that the higher charge and smaller size distribution particles are less likely to form aggregates. In the present work, DLS measurements were carried out in the presence of 0.01 M of KCl to confirm the accurate particle size. DLS measurement of magnetite coated with RK/amidoxime indicated that the size was 45 nm and polydispersity index (PDI) is 0.098. DLS data showed larger particle size than TEM, which may be caused by the mutual magnetic interaction of the particles to form some magnetic aggregates, thus disturbing DLS [29]. The data indicated that magnetite diameter increased with coating with RK/amidoxime and PDIs decreased and became monodisperse. It can be concluded that the encapsulation of a high amount of magnetite and formation of bilayer adsorption of RK/ amidoxime at magnetite surfaces can influence the chemical stability of particles.

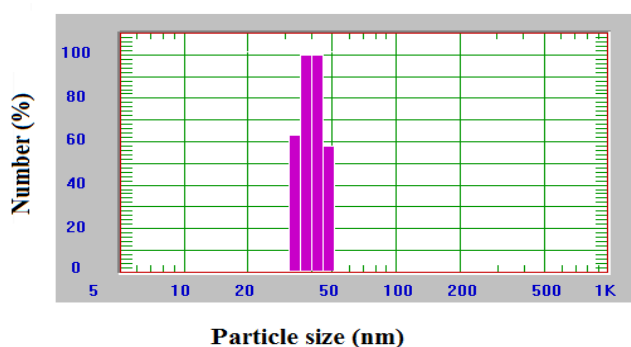


**Figure 3.** DLS measurements of magnetite-RK/amidoxime nanoparticles in 0.01 M KCl at 25 °C.

### 3.3 Polarization studies

Figure 4 shows the typical cathodic and anodic Tafel polarisation curves for steel in 1 M HCl solution in the absence and presence of different concentrations of magnetite-RK/amidoxime nanoparticles. From the polarization curves, it can be obviously seen that the addition of magnetite-RK/amidoxime nanoparticles to the solution significantly retarded both cathodic (hydrogen evolution) and anodic reactions (steel dissolution). Obviously, the cathodic and anodic Tafel slope values in the presence of inhibitor have changed with respect to the blank solution. The results revealed that the addition of magnetite-RK/amidoxime nanoparticles functioned by blocking the active anodic and cathodic inhibition of both the sites. Therefore, magnetite-RK/amidoxime nanoparticles can be classified as mixed-type inhibitor [30-32]. The inhibition action of magnetite-RK/amidoxime nanoparticles was more pronounced at higher concentration. Moreover, the polarization curves shifted toward lower corrosion current densities ( $I_{corr}$ ) and less negative corrosion potentials ( $E_{corr}$ ) in the presence of magnetite-RK/amidoxime nanoparticles. In the presence of inhibitor, a protective layer might be formed on the surface, blocking the active sites and modifying the surface condition. This would lead to the shift of anodic and/or cathodic branches toward lower current densities [33]. The addition of magnetite-RK/amidoxime nanoparticles produces a negative shift in the  $E_{corr}$  values which is an indication of the interaction of the magnetite-RK/amidoxime nanoparticles with steel surface [4]. Further, there has not been much change in the  $E_{corr}$  of the inhibited test solutions indicating the mixed nature of the inhibitor, which prevents both anodic and cathodic reactions. It is further confirmed by the variation of  $ba$  and  $bc$  values of blank solution from that of the inhibited solution. These results suggest that in the presence of magnetite-RK/amidoxime nanoparticles, a protective film gets adsorbed onto the steel substrate impeding the dissolution of steel in anodic sites and slows down the cathodic reactions.

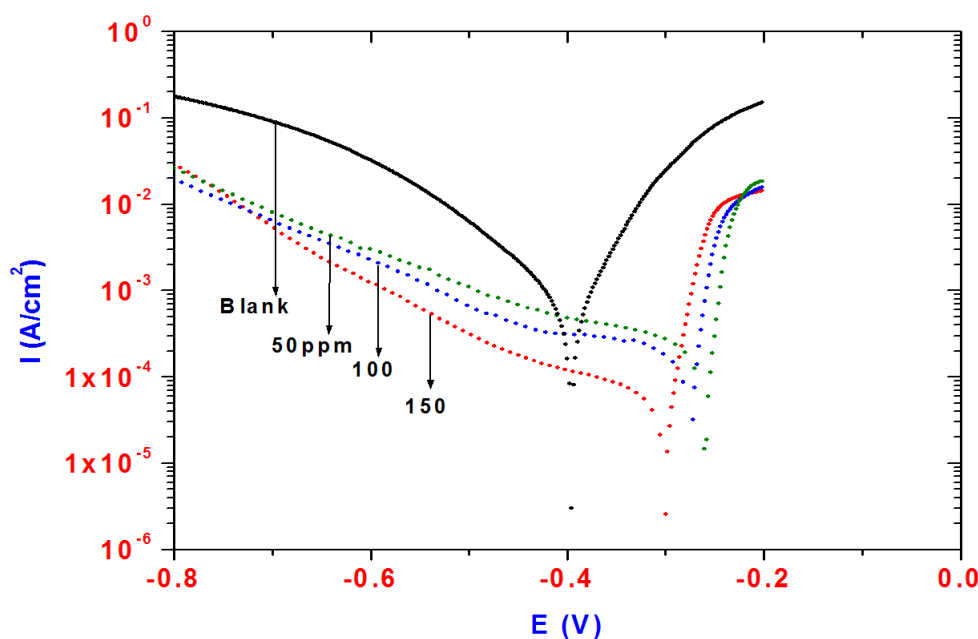


**Figure 4.** Polarization curves for steel in 1M HCl solution containing Myrrh with different concentrations

The results can be accounted to the covering of the surface with magnetite-RK/amidoxime nanoparticles. The anodic dissolution of steel and the cathodic reduction of hydrogen are arrested with the barrier created at the steel/solution interface. So, both anodic and cathodic processes are inhibited in the presence of inhibitor indicating that magnetite-RK/amidoxime nanoparticles acts as mixed type inhibitor. The obtained values of electrochemical parameters such as corrosion potential, ( $E_{corr}$ ), corrosion current density ( $i_{corr}$ ), anodic ( $b_a$ ) and cathodic ( $b_c$ ) Tafel slopes are given in Table 1.

**Table 1.** Inhibition efficiency values for steel in 1M HCl with different concentrations of Myrrhyh calculated by Polarization and EIS methods.

	Polarization Method					EIS Method		
	Ba (mV)	Bc (mV)	$E_{corr}$ (V)	$i_{corr}$ ( $\mu A/cm^2$ )	IE%	$R_p$ Ohm	Cdl ( $\mu F/cm^2$ )	IE%
Blank	69	120	-0.3955	839	_____	1.80	334	_____
50ppm	26	276	-0.2610	168	79.9	9.2	139	80.4
100	30	222	-0.2750	91	89.1	19.2	106	90.6
150	34	165	-0.3029	28	96.6	57	101	96.8

The corrosion inhibition efficiency is evaluated from the corrosion current densities values using the relationship [34-36]:

$$\% IE = \frac{i_{corr} - i_{corr(inh)}}{i_{corr}} \tag{1}$$

where  $i_{corr}$  and  $i_{corr(inh)}$  are the values of corrosion current density of uninhibited and inhibited specimens, respectively. The inhibition efficiency (IE%) calculated from the potentiodynamic polarization curves are presented in Table 1. The increase in inhibition efficiency with increasing concentrations of inhibitor may be attributed to an increase in the surface coverage of inhibitor on steel surface. In addition, the inhibition efficiency of the inhibitor by polarization curves exhibited the maximum inhibition efficiency (96.6%) at the highest concentration of 150ppm. It can be concluded that the presence of magnetite-RK/amidoxime nanoparticles prevented the attack of acid medium on steel surface.

### 3.4. Electrochemical impedance spectroscopy (EIS)

Figure 5 represents the Nyquist diagrams for the steel in 1 M HCl in the absence and presence of magnetite-RK/amidoxime nanoparticles. It is clear that the impedance spectra exhibit a capacitive loop. The diameter of the capacitive loop in the presence of inhibitor is bigger than that in the absence

of inhibitor (blank solution) and increases with the inhibitor concentration. This implies that corrosion of steel in 1 M HCl solution is mainly controlled by charge transfer process [37–41]. Noticeably, these capacitive loops are not perfect semicircles which can be attributed to the frequency dispersion effect as a result of the roughness and in-homogeneous of the electrode surface [13]. The EIS data were analyzed by fitting to the equivalent circuit model shown in Fig. 6. The circuit comprises a solution resistance ( $R_s$ ), charge transfer resistance ( $R_{ct}$ ) and constant phase element (CPE). It is worth mentioning that the double layer capacitance ( $C_{dl}$ ) value is affected by imperfections of the surface, and that this effect is fitted using a constant phase element (CPE) [42]. The impedance of the CPE is expressed by the following expression:

$$Z_{CPE} = Y_0^{-1} (j\omega)^{-n} \tag{3}$$

where  $Y_0$  is a proportional factor,  $j^2 = -1$  is an imaginary number, and  $\omega$  is the angular frequency ( $\omega = 2\pi f$ ). Depending on the value of  $n$ , CPE can represent an inductance ( $Z_{CPE} = L, n = -1$ ), a resistance ( $Z_{CPE} = R, n = 0$ ), and a Warburg impedance ( $Z_{CPE} = W, n = 0.5$ ). If  $n = 1$ , the impedance of CPE is identical to that of a capacitor, and in this case  $Y_0$  gives a pure capacitance ( $C$ ). The impedance parameters of  $R_s, R_{ct}, C_{dl}$  are presented in Table 1. The inhibition efficiency values (IE%) were calculated from  $R_{ct}$  data using the following equation:

$$IE\% = 1 - \frac{R_{ct(1)}}{R_{ct(2)}} \times 100 \tag{3}$$

where  $R_{ct(1)}$  and  $R_{ct(2)}$  are the charge transfer resistances in the HCl solution in the absence and in the presence of the inhibitors, respectively. Clearly,  $R_{ct}$  value increases prominently, while  $C_{dl}$  reduces with the concentration of inhibitor. A large charge transfer resistance is associated with a slower corroding system.

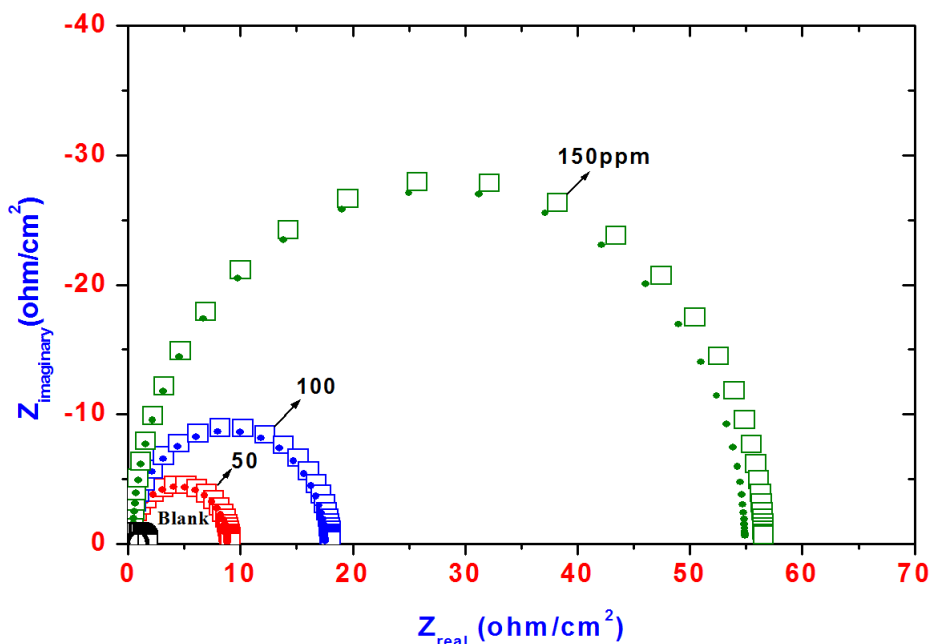


**Figure 6.** Nyquist diagram for steel in 1 M HCl solution containing Myrrh with different concentrations showing experimental (square) and fitted data (circle).

It is known that  $R_{ct}$  is reciprocally proportional to the corrosion rate [43]. The values of charge transfer resistance  $R_{ct}$  increase with rise of concentration, which indicates the formation of the insulated adsorbed layer on the steel surface. The decrease in  $C_{dl}$  value can be attributed to a decrease in local dielectric constant and/or an increase in the thickness of electrical double layer [44]. The double layer between the steel surface and the solution is considered as an electrical capacitor. The adsorption of magnetite-RK/amidoxime nanoparticles on the steel surface decreases its electrical capacity because they displace the water molecules originally adsorbed on the surface [45-46]. The presented data in Table1 show that, the inhibiting efficiency increases, with inhibitor concentration reaching 96.8% for 250ppm. The inhibiting efficiency values got from EIS data are comparable and run parallel with those obtained from the potentiodynamic polarization measurements.

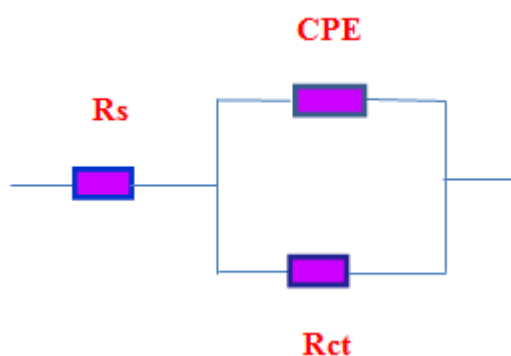


**Figure 7.** Equivalent circuit employed for fitting the EIS data.

#### 4. CONCLUSIONS

1. Magnetite-RK/amidoxime nanoparticles acts as a good corrosion inhibitor for steel in 1 M HCl.
2. Results of polarization studies suggest that magnetite-RK/amidoxime nanoparticles -behaves as a mixed type inhibitor.
3. EIS spectra exhibit a capacitive loop and its diameter increases with magnetite RK/amidoxime nanoparticles concentration. The presence of magnetite-RK/amidoxime nanoparticles in 1 M HCl solution increases the charge transfer resistance ( $R_{ct}$ ) while reduces the double layer capacitance ( $C_{dl}$ ).
4. The inhibiting efficiency values got from EIS data are comparable and run parallel with those obtained from the potentiodynamic polarization measurements.

#### ACKNOWLEDGEMENT

The authors extend their appreciation to the Deanship of Scientific Research at King Saud University for funding this work through research group no RGP-VPP-235.

## References

1. L.T. Popoola<sup>1</sup>, A.S. Grema, G. K. Latinwo, B. Gutti A. S. Balogun, *Int. J. Ind. Chem.* 4 (2013) 35
2. V. S Sastri. Green Corrosion Inhibitors. Theory and Practice. John Wiley & Sons: Hoboken, NJ; 1998.
3. Y. Xia, and G.M. Whitesides, "Soft Lithography", *Angewandte Chemie International Edition*, vol., no. 5, pp. 550–575, 1998.
4. G.K. Jannings, T.H. Yong, J.C. Munro, and P.E. Laibinis, *J. Amer. Chem. Soc.*, 125 (2003) 2850.
5. A. Ulman, *Chem. Rev.*, 96 (1996) 1533.
6. A. M. Atta, O. E. El-Azabawy, H.S. Ismail, M.A. Hegazy, *Corros. Sci.* 53 (2011) 1680.
7. AM. Atta, G A. El-Mahdy, H A. Al-Lohedan and A. O. Ezzat *Molecules* 19 (2014) 10410.
8. A M. Atta, G A. El-Mahdy, H A. Al-Lohedan and Sami A. Al-Hussain *Int. J. Mol. Sci.* 15 (2014) 6974.
9. G. A. El-Mahdy, A.M. Atta and H. A. Al-Lohedan, *Molecules* 19 (2014) 1713.
10. G. A. El-Mahdy, A. M. Atta, H. A. Al-Lohedan *J.TAIWAN. INST. CHEM. E.* 45 (2014) 1947
11. A M. Atta<sup>1</sup>, G A. El-Mahdy<sup>1,3</sup>, H A. Al-Lohedan<sup>1</sup> and S A. Al-Hussain, *Int. J. Electrochem. Sci.*, 9 (2014) 8446.
12. A M. Atta<sup>1</sup>, G A. El-Mahdy, H A. Al-Lohedan<sup>1</sup> and A. O. Ezzat, *Int. J. Electrochem. Sci.*, 9 (2014) 8226 .
13. A M Atta GA El-Mahdy H S. Ismail<sup>2</sup> and H A. Al-Lohedan, *Int. J. Electrochem. Sci.*, 7 (2012) 11834 – 11846
14. A. M. Atta G. A. El-Mahdy, A. K. F. Dyab, and Hamad A. Allohedan, *Int. J. Electrochem. Sci.*, 8 (2013) 9629 – 9643
15. G. A. El-Mahdy , A. M Atta and H. A. Al-Lohedan, *Int. J. Electrochem. Sci.*, 8 (2013) 5052 – 5066
16. A. M. Atta, I. F. Nassar, H. M. Bedawy *React. Func. Polym.*, 67(2007) 617
17. Ayman M. Atta, Shymaa M. El-Saeed, Reem K. Farag *React. and Func. Polym.*, . 66, .( 2006), 1596.
18. Ayman M. Atta, Ashraf M. Elsaheed, Reem K. Farag, Shymaa M. El-Saeed *React. Func. Polym.*,67 (2007) 549.
19. A. M. Atta, R. Mansour, M. I. Abdou and A. M. El-Sayed, *J. Polym. Res.* 12 (2005)127
20. J.H. Wills, A.M. Kunkel, R.V. Brown, G.E. Science 125 (1957) 743.
21. B.M. Askew, , *Brit. J. Pharmacol.* 13 (1958) 202.
22. T. Diem a, W. Fabianowski a, R. Jaccodine b, R. Rodowski, *Thin Solid Films* 265 (1995) 71
23. B. Muller, G. Kubitzki, G. Kinet, *Corros. Sci.* 40 (1998) 1469–1477.
24. L. Xianghong D. Shuduan , X. Xiaoguang Xie *Corros. Sci.* 81 (2014) 162.
25. B. Muller, G. Kubitzki, G. Kinet. *Corros. Sci.* 40 ( 1998) 1469 .
26. I. Bicu, F. Mustata, *J. Polym. Sci.: Part A: Polym. Chem.* 43(2005) 6308-6322.
27. A M. Atta, H A. Al-Lohedan and S A. Al-Hussain *Molecules* 19 (2014) 11263.
28. F. Arranz, M. Sanchez-Chaves, M. M. Gallego, *Angew. Makrom. Chem.* 218 (1994) 183.
29. M. A Ali A. M Atta, A.M Yousef and M. Alaa *Poly. Intern.* 62, (2013) 1667. 30. S.
30. Garcia, T. Muster, O. Ozkanat, N. Sherman, A. Hughes, H. Terryn, *Electrochim. Acta* 55 (2010) 2457.
31. Y. Yan, W. Li, L. Cai, B. Hou, *Electrochim. Acta* 53 (2008) 5953.
32. K. Khaled, *Electrochim. Acta* 48 (2003) 2493.
33. H. Ashassi, D. Ghasemi, *Appl. Surf. Sci.*, 249 (2005) 408.
34. Q. Qu, Z. Hao, L. Li, W. Bai, Z. Ding, *Corros. Sci.* 51 (2009) 569.
35. F. Bentiss, M. Lebrini, M. Lagrenée, *Corros. Sci.* 47 (2005) 2915.
36. Q. Qu, S. Jiang, W. Bai, L. Li, *Electrochim. Acta* 52 (2007) 6811.
37. M. Erbil M.. *Chim Acta Turc* 1(1988)59.

38. I. Dehri , H. Sozusag, M. Erbil . *Prog Org Coat* 48 (2003)118.
39. F. Bentiss, B. Mernari, M. Traisnel, H. Vezin, M. Lagrenee. *Corros Sci* 53 (2011)487.
40. A. Chetouani , A. Aouniti, B. Hammouti , N. Benchat, T. Benhadda, S. Kertit *Corros Sci.* 45 (2003)1675.
41. M. Ozcan , I. Dehri , M. Erbil . *Appl Surf Sci.* 236 (2004)155.
42. M. Lebrini, M. Lagrene'e, H. Vezin, M. Traisnel, F. Bentiss *Corros Sci* 49 (2007)2254.
43. S. Cheng, J. Tian, S. Chen, Y. Lei, X. Chang, T. Liu, Y. Yin, *Mater. Sci. Eng. C* 29 (2009) 751.
44. M.A. Amin, Khaled KF, Fadi-Allah SA. *Corros Sci* 52 (2010)140.
45. G. Avci., *Mater Chem Phys* 112 (2008) 234.
46. KF Khaled. *Mater Chem Phys* 112 (2008) 290.

© 2015 The Authors. Published by ESG ([www.electrochemsci.org](http://www.electrochemsci.org)). This article is an open access article distributed under the terms and conditions of the Creative Commons Attribution license (<http://creativecommons.org/licenses/by/4.0/>).